Advances in validating gyrokinetic turbulence models against L- and H-mode plasmas

Advances in validating gyrokinetic turbulence models against L- and H-mode plasmas[a)]

C. Holland,[1,b)] L. Schmitz,[2] T. L. Rhodes,[2] W. A. Peebles,[2] J. C. Hillesheim,[2] G. Wang,[2] L. Zeng,[2] E. J. Doyle,[2] S. P. Smith,[3] R. Prater,[3] K. H. Burrell,[3] J. Candy,[3] R. E. Waltz,[3] J. E. Kinsey,[3] G. M. Staebler,[3] J. C. DeBoo,[3] C. C. Petty,[3] G. R. McKee,[4] Z. Yan,[4] and A. E. White,[5]
[1]*University of California-San Diego, 9500 Gilman Drive, La Jolla, California 92093-0417, USA*
[2]*University of California-Los Angeles, PO Box 957099, Los Angeles, California 90095-7099, USA*
[3]*General Atomics, PO Box 85608, San Diego, California 92186-5608, USA*
[4]*University of Wisconsin-Madison, 1500 Engineering Dr., Madison, Wisconsin 53706, USA*
[5]*Massachusetts Institute of Technology, 77 Massachusetts Ave., Cambridge, Massachusetts 02139, USA*

(Received 22 December 2010; accepted 15 March 2011; published online 9 May 2011)

Robust validation of predictive turbulent transport models requires quantitative comparisons to experimental measurements at multiple levels, over a range of physically relevant conditions. Toward this end, a series of carefully designed validation experiments has been performed on the DIII-D tokamak [J. L. Luxon, Nucl. Fusion **42**, 614 (2002)] to obtain comprehensive multifield, multipoint, multiwavenumber fluctuation measurements and their scalings with key dimensionless parameters. The results of two representative validation studies are presented: an elongation scaling study performed in beam heated L-mode discharges and an electron heating power scan performed in quiescent H-mode (QH-mode) discharges. A 50% increase in the elongation κ is observed to lead to a ~50% increase in energy confinement time τ_e and accompanying decrease in fluctuation levels, qualitatively consistent with *a priori* theoretical predictions and nonlinear GYRO [J. Candy and R. E. Waltz, J. Comput. Phys. **186**, 545 (2003)] simulations. However, these simulations exhibit clear quantitative differences from experiment in the predicted magnitudes and trends with radius of turbulent fluxes and fluctuation levels which cannot be fully accounted for by uncertainties due to transport stiffness. In the QH-mode study, local nonlinear GYRO simulations that neglect fast ion effects show a similar proportional response to the applied electron cyclotron heating as the experiment, but overpredict the magnitudes of transport and fluctuation levels by a factor of 10 or more. Possible sources of this overprediction, namely nonlocal effects and self-consistent fast beam ions, are identified and discussed. © *2011 American Institute of Physics*. [doi:10.1063/1.3574518]

I. INTRODUCTION

The transport of particles, energy and momentum by gyroradius-scale microturbulence, is a key determinant of plasma confinement in magnetic confinement based fusion devices.[1] Developing a quantitatively accurate predictive capability for this transport is therefore essential to improve our ability to design and explore future reactor-relevant devices and for interpreting results from current-day experiments. While there is a complex array of physics involved in the dynamics of plasma microturbulence, significant progress has been made in developing first principles based computational models that make predictions of both these turbulent fluxes and the statistics of underlying turbulence characteristics such as amplitudes and spectra. The question now becomes one of the model validation:[2–5] assessing how well these theoretical and computational models can in fact quantitatively predict the actual, experimentally measured turbulence and transport in various discharges and conditions. While there is a long history of testing various transport predictions against independent power balance modeling calculations[6,9] (often termed the experimental fluxes even though they are not directly measured), the coupling of these tests with simultaneous quantitative tests of predicted fluctuation characteristics is a much more recent phenomenon,[8–16] owing equally to advances in experimental diagnostic capabilities, in theoretical model complexity, and in computational capability to solve these increasingly complex models. However, these multilevel tests of model predictions (i.e., at multiple levels of the validation hierarchy[4]) are essential for establishing confidence in our understanding of the fundamental underlying physics of turbulent transport and our ability to accurately extrapolate to future regimes.

In this paper, results from two validation studies are presented, in which the fidelity of the so-called local, "δf," gyrokinetic-Maxwell[17–19] equations (described further in Sec. III) in predicting microturbulence levels and the associated transport is examined. The GYRO code[7,20,21] is used to solve these nonlinear equations and to calculate the predicted transport and turbulence characteristics. In the first study, we assess the ability of this theoretical model to predict turbulence and transport levels in a pair of low confinement (L-mode) DIII-D discharges in which the plasma elongation

[a)]Paper NI2 5, Bull. Am. Phys. Soc. **55**, 193 (2010).
[b)]Invited speaker.

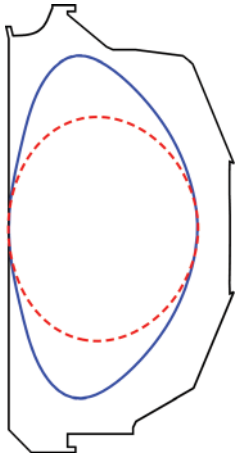

FIG. 1. (Color online) Contours of the last closed flux surfaces for DIII-D discharges 136674 ($\kappa = 1.8$) (solid) and 136693 ($\kappa = 1.2$) (dashed), time-averaged over the period of 1280–1480 ms.

κ was varied by 50% (from separatrix values of 1.2 to 1.8). This study was motivated by previous theoretical research using GYRO,[22] which made a clear prediction of strongly improved confinement and decreasing transport as the elongation is increased (while all other dimensionless parameters are held fixed); this prediction was borne out in the experiment. Simulations using actual discharge profiles and conditions predict a corresponding decrease in transport and turbulence with increased elongation that is roughly consistent with the measured changes. However, there are clear differences in magnitudes and radial trends between the model predictions and experimental measurements. Assessments of the uncertainties in these predictions using sensitivity analyses, comparisons of flux-gradient relationships, and calculation of transport solution profiles (defined in Sec. IV) using the quasilinear TGLF transport model[23,24] indicate that some discrepancies are larger than plausible uncertainties in the results due to bias or likely systematic uncertainties in the experimental profile fits. Also, initial results are presented from a comparison of GYRO predicted fluxes and fluctuations in a pair of low density quiescent H-modes,[25,26] in which the electron heating power was varied by adding 2.8 MW of electron cyclotron heating (ECH) to a base case scenario with 6.9 MW of neutral beam heating. While the GYRO calculations predict turbulent fluxes that respond in a similar fashion as the experiment to the added ECH power and corresponding profile changes, they overpredict the power balance fluxes by 1 to 2 orders of magnitude. A survey of physics effects not included in these initial simulations identifies nonlocality and a self-consistent treatment of fast beam ions as the likely missing components necessary to bring the gyrokinetic predictions and power balance calculations into agreement.

II. L-MODE ELONGATION SCAN EXPERIMENTAL CONDITIONS

The discharges used in this validation study were carefully designed with an eye toward optimization for validation purposes, rather than peak performance or exotic behavior. This goal translates into considering stationary (or at best slowly evolving) plasmas that exhibit no macroscopic or magnetohydrodynamic (MHD) instabilities such as sawteeth, tearing modes, or Alfvén waves, which are not included in the turbulence models and would thus complicate the analysis. Furthermore, significant integration times are necessary to obtain well-converged measurements of fluctuation statistics. These conditions are met by taking data averaged over 200 ms from the slowly evolving presawtooth phase of a pair of inner wall limited, neutral beam heated L-mode discharges.

Contours of the equilibrium flux surfaces are shown in Fig. 1 and time-averaged equilibrium profiles in Fig. 2. The density profiles were measured via reflectometry, the electron temperature profiles via electron cyclotron emission (ECE), and ion profiles via charge exchange recombination spectroscopy (CER); motional Stark effect measurements were used in constraining the equilibrium reconstructions. The use of a 200 ms averaging window in this slowly evolving phase yields very small (<5%) statistical uncertainties in the profiles, smaller generally than the thickness of the plotted curves and so are not plotted. While significantly harder to quantify, the possibility of systematic uncertainties or errors due to, e.g., diagnostic calibration errors, analyst choices in profile fitting settings, or in the calculation of the magnetic equilibrium used in the profile fitting must also be kept in mind when comparing

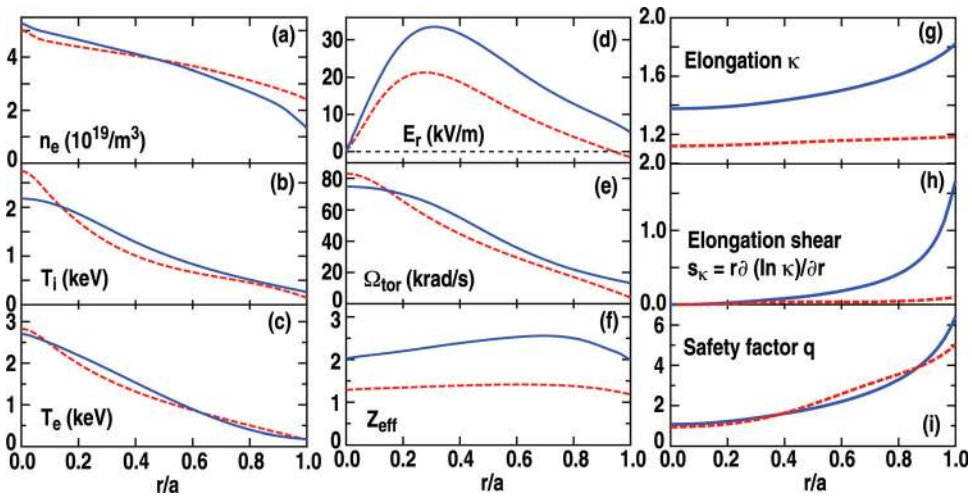

FIG. 2. (Color online) Equilibrium profiles for DIII-D discharges 136674 (solid) and 136693 (dashed), averaged from 1280 to 1480 ms: (a) electron density n_e, (b) ion temperature T_i, (c) electron temperature T_e, (d) radial electric field E_r, (e) torodial rotation Ω_{tor}, (f) $Z_{eff} = \sum_i Z_i^2 n_i / \sum_i Z_i n_i$, (g) elongation κ, (h) elongation shear $s_\kappa = r\partial(\ln\kappa)/\partial r$, and (i) safety factor q.

profiles. The impact of such errors is discussed further in Sec. IV. These plasmas were run with on-axis toroidal field $B_T = 2.1$ T, plasma current $I_p = 1.15$ MA, line-averaged density $\overline{n_e} = 3.2 \times 10^{19}/\mathrm{m}^3$, on-axis temperatures of 2–3 keV, and $\beta_N = \beta(aB/I_p) = 0.65$ [where $\beta = \langle p \rangle / (B^2/2\mu_0)$ is the normalized plasma pressure, B is the total magnetic field strength, a is the plasma minor radius, and I_p is the plasma current] in the high elongation discharge ($\kappa = 1.8$ at $r/a = 1$, where r/a denotes normalized toroidal flux). Corresponding values for the low elongation ($\kappa = 1.2$ at $r/a = 1$) case are $I_p = 0.7$ MA, $\overline{n_e} = 4.1 \times 10^{19}/\mathrm{m}^3$, and $\beta_N = 1.45$.

Consistent with the motivating theoretical predictions and previous experimental results,[27] an increase in the energy confinement time τ_E from 50 ms in the low κ case to 80 ms in the high κ case is observed. More directly, twice the heating power (two neutral beam sources) was required in the low κ case to maintain profiles similar to those obtained with a single neutral beam source in the high κ case. It should be noted that there is a strong change in the plasma current I_p as well as the elongation, which is also well known to have a strong impact on plasma confinement.[28] Such a variation is necessary in order to maintain consistency in the (dimensionless) safety factor q ($= rB_\phi/RB_\theta$ in a circular plasma) between the two shapes. While the aim of this experiment was not to conduct a perfect dimensionless scaling[29] experiment *per se*, it was designed to minimize variations as much as possible in the profiles of dimensionless parameters upon which the local gyrokinetic model depends and which motivating theoretical predictions assumed were held fixed.

Also consistent with the theoretical expectations was the rise in observed long-wavelength fluctuation levels, shown in Fig. 3. Density fluctuations (normalized to the local equilibrium density level) measured via beam emission spectroscopy (BES)[30] exhibited up to a factor of 3 increase in root mean square (RMS) amplitude with decreased elongation. Long-wavelength electron temperature fluctuation amplitudes (also locally-normalized) measured with correlation electron cyclotron emission (CECE) radiometry[31] exhibit a smaller but still clear increase in fluctuation amplitude with decreased elongation. The BES diagnostic is sensitive to fluctuations with $k_\theta < 3\,\mathrm{cm}^{-1}$ and the CECE diagnostic to fluctuations with $k_\theta < 2\,\mathrm{cm}^{-1}$. Typical values of ρ_s in L-mode plasmas are on the order of a few millimeters, such that these ranges roughly correspond to $k_\theta \rho_s < 1$, the range in which the ion temperature gradient (ITG) and trapped electron mode (TEM) instabilities are generally found to dominate.

III. GYRO SIMULATIONS OF ELONGATION SCAN DISCHARGES

While these experimental results support the motivating theoretical predictions in a qualitative sense and go beyond the previous experiments in quantifying the response of fluctuations as well as confinement to the changes in elongation, the question of quantitative consistency with the gyrokinetic turbulence model remains. In order to quantitatively test the model, simulations using the measured profiles and corresponding dimensionless parameters (all of which vary to some degree between the two discharges, not simply the elongation) must be performed. The GYRO code is used to make these predictions for two reasons. The first is to be consistent with the motivating work and the second is because of the breadth of physics it encompasses, much of which has been shown to be necessary for quantitatively accurate modeling of real plasmas.[7] GYRO is a nonlinear, continuum, initial value code that solves the δf version of the gyrokinetic-Maxwell equations.[17–19] That is, it describes the dynamics of small fluctuations δf of the ion and electron distribution functions around a large, constant Maxwellian background distribution f_0. The simulations described in this paper include equilibrium rotation and $\vec{E} \times \vec{B}$ shear flow effects (self-consistently calculated from the experimentally measured rotation profiles), incorporate magnetic shaping effects through use of the Miller equilibrium model,[32] and describe dynamic ion species using the full gyrokinetic equation, but treat electron dynamics using the drift-kinetic equation. Pitch-angle scattering of the electrons due to electron-electron and electron-ion collisions is also included. Throughout this paper, we refer to ion species whose dynamics are self-consistently calculated via the gyrokinetic equation to be dynamic, as opposed to those which might be either treated as adiabatic or simply ignored (such as nonfully ionized carbon ions, or the "fast" deuterium ions generated by the neutral beams). The simulations are also performed in the local (sometimes called flux-tube) GYRO operation mode, in

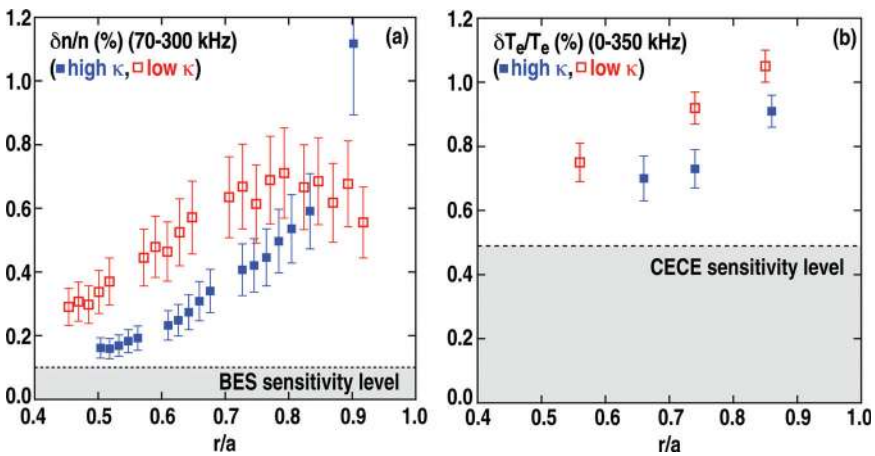

FIG. 3. (Color online) Root mean square locally normalized (a) density fluctuation amplitudes measured via BES and (b) electron temperature fluctuation amplitudes measured via CECE. Measurements from the high κ discharge (136674) are plotted as solid squares and from the low κ discharge (136693) as open squares.

which a rigorous $\rho* = \rho_s/a \rightarrow 0$ limit of the δf gyrokinetic-Maxwell equations is solved ($\rho_s = c_s/\Omega_{ci}$, $c_s = \sqrt{T_e/M_i}$, $\Omega_{ci} = eB/M_i c$, and a is the midplane minor radius of the plasma). This local limit exploits the assumed scale separation between fluctuation and equilibrium spatiotemporal scales used in the derivation of the δf model [typical values of $\rho* = O(10^{-3})$ in these plasmas] to simplify the numerics and corresponds to a physical assumption that the properties of the turbulence and transport at a given flux surface only depend upon the local dimensionless parameters at that surface. Comparisons with nonlocal simulations (which relax this assumption by including the spatial variations of the dimensionless parameters) will also be described below.

It is also appropriate to note at this point that before any meaningful model validation can be done using a complex numerical code such as GYRO, a comprehensive verification[2–5] of that code must be performed. Verification is the process of assessing how well a given numerical or computational code solves the intended mathematical model, without reference to the physical relevance of that mathematical model. That is, verification quantifies the accuracy to which a given code solves the intended model equations, and validation assess whether those equations adequately describe the experimentally observed phenomena of interest. The extensive successful verification of linear and nonlinear GYRO predictions against both analytic theory and other codes (as documented in Ref. 21) is another motivation for its use in these validation studies.

A. Identification of key physics via analysis of linear growth rates

A challenge for any computationally intensive (and often resource limited) validation exercise is to identify what physical phenomena are expected to make a strong impact on model predictions and to what physics the model predictions should be insensitive to. For turbulent transport model validation, an efficient way of conducting an initial assessment of the key physics is to quantify the responses of linear growth rates to the inclusion of different physics components. Because of the strong correlation expected between linear growth rates, nonlinear saturation levels of the turbulence, and the corresponding fluxes, assessing the sensitivities of growth rates (which can be calculated much more easily than fully nonlinear simulations) is an optimal way to begin a validation study.

The results of such an analysis are shown in Fig. 4, where the linear growth rates of fluctuations over the range of poloidal mode numbers $0 \leq k_\theta \rho_s \leq 1.2$ (where $k_\theta = nq/r$, with n being the toroidal mode number, q the safety factor, and r the midplane minor radius) are shown as a function of increasing physical complexity, for both the low and high κ cases at $r/a \sim 0.75$. The plotted growth rates are for the fastest growing modes as calculated by GYRO. The instabilities in the low κ shape are typically ion modes (in that they have phase velocities in the ion diamagnetic direction), while the high κ instabilities are electron modes. In both cases, inclusion of (drift-)kinetic electrons can yield over a factor of 2 increases in growth rate (even in the low κ case, where the fastest growing instabilities remain ion modes) relative to the adiabatic electron case. The magnitude of this effect calls into question the ability of models that use adiabatic electrons to make quantitatively relevant predictions of near-edge turbulence, particularly in shaped plasmas where the equilibrium $\vec{E} \times \vec{B}$ shear rate $\gamma_{\vec{E}\times\vec{B}}$ can be half the peak adiabatic electron growth rate. Shearing rates of these magnitudes often lead to strong, if not total, suppression of the turbulence.

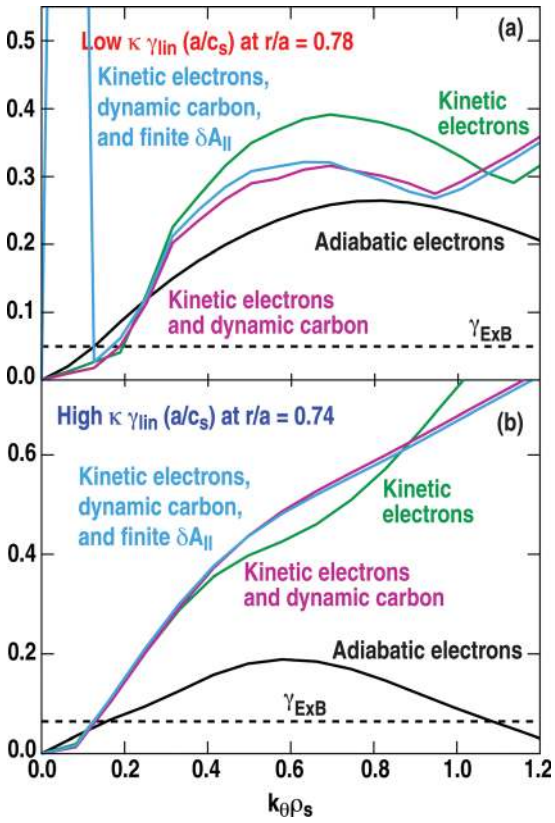

FIG. 4. (Color) Comparison of linear growth rates for the (a) low κ and (b) high κ discharges as a function of increasing physical complexity. Growth rates calculated using only adiabatic electrons (black), kinetic electrons (green), kinetic electrons and dynamic carbon ions (magenta), and kinetic electrons, dynamic carbon ions, and finite $\delta A_{||}$ (cyan). The local $\vec{E} \times \vec{B}$ shearing rate is plotted as a dashed black line for reference.

The next strongest effect is found to be the inclusion of dynamic carbon impurity ions, which are typically "lumped in" with the thermal deuterium ion distribution, and simply represented via inclusion of the experimental $Z_{eff} > 1$ in the calculation of collision rates. A fully self-consistent treatment via solution of the gyrokinetic equation for δf_{carbon} in addition to the bulk thermal deuterium fluctuations $\delta f_{deuterium}$ is found to stabilize the low κ ion modes and high κ electron modes at higher k_θ, but destabilize the low k_θ electron modes in the high κ plasma. Perhaps more intriguing is that the larger response is seen in the low κ case, which has a lower Z_{eff} (1.4) than in the high κ case ($Z_{eff} \sim 2.4$). Based upon these results, both drift-kinetic electrons and fully self-consistent carbon ions are included in all the GYRO simulations discussed in this paper.

In contrast to the inclusion of kinetic electrons and dynamic carbon ions, including electromagnetic ($\delta\vec{B}_\perp = \vec{\nabla} \times \delta A_{||} \neq 0$, $\delta B_{||} = 0$) fluctuations have virtually no

impact on the growth rates at these locations. The inclusion of electromagnetic effects can, however, lead to numerical issues when combined with finite electron collisions for typical GYRO grid resolutions, manifesting as unphysical modes with large frequency and growth rate at long wavelength; an example is the spike at low k_θ in the electromagnetic growth rate calculation of the low κ case [Fig. 4(a)]. This instability can be eliminated by use of increased resolution in the collision operator. However, because electromagnetic effects are expected to be small at most of the radii of interest for this study, we circumvent the issue by considering only electrostatic simulations run with standard resolution. Preliminary linear and nonlinear investigations indicate that finite electromagnetic effects do have a non-negligible stabilizing effect at smaller radii, due to larger β values relative to the larger radii where the fluctuation measurements were obtained.

B. Comparison of GYRO predicted fluxes against power balance results

Having identified the (expected) key physics via the linear growth rate analysis of Sec. III A, a series of nonlinear local GYRO simulations has been carried out to test the ability of GYRO to predict the turbulent transport in these discharges. These simulations were conducted at a five different radial locations spanning the plasma, weighted toward the outer r/a where measurements of turbulent fluctuations are also available. Typically, simulation box sizes are $L_x = L_y = 100\ \rho_s$ at large r/a to 80 ρ_s at smaller r/a, where L_x and L_y are the radial and binormal simulation domain sizes, respectively. Twenty or more toroidal modes were used to span the range $0 \leq k_\theta \rho_s \leq 1.2$ to 1.4, with a higher maximum $k_\theta \rho_s$ required for simulations at $r/a = 0.65$ and 0.75 in the high κ discharge. A standard 128-point velocity space discretization is used: eight pitch angles, eight energies, and two signs of velocity. Time integration is done with a fixed timestep implicit/explicit Runge-Kutta scheme, coupled with fourth-order Runge-Kutta integration of the nonlinear terms. Integration timesteps h range from 0.005 (at large r/a) to 0.02 a/c_s (at small r/a).

Typical time histories of the ion and electron energy fluxes $Q_{i,e} = 1.5\langle \tilde{p}_{i,e} \tilde{v}_r \rangle$ (where the brackets denote a magnetic flux surface average, $\tilde{p}$ is the pressure fluctuation, and $\tilde{v}_r$ is the radial velocity fluctuation) are shown in Fig. 5. Each simulation was run for several hundred a/c_s in a saturated state and then time-averaged to calculate the mean predicted flux levels that will be compared against the power balance results. In order to assess the statistical uncertainty of these results, an ensemble of flux estimates is generated by averaging over consecutive 50 a/c_s intervals (to average over the fast inherent variability of the turbulence, with decorrelation rates on the order of 10 a/c_s). The standard deviation of the mean of this ensemble is taken to provide a representative estimate of the statistical uncertainties. In practice, it is found that the simulations were run sufficiently long for these uncertainties to be on the order of 10% or less, and thus small compared to expected systematic uncertainties due to uncertainties in the input parameters such as local scale lengths. For instance, this procedure estimates the statistical uncertainties in the simulation shown in Fig. 5 as $Q_i = 1.27 \pm 0.03$ W/cm^2 and $Q_e = 2.01 \pm 0.03$ W/cm^2. This level of statistical convergence was achieved by running each simulation with 64 processors per toroidal mode (thus 1280 processors for a typical 20-mode simulation) for 12–14 hours on the "jaguar" Cray XT5 machine, such that each simulation required in total 15 000–20 000 processor-hours.

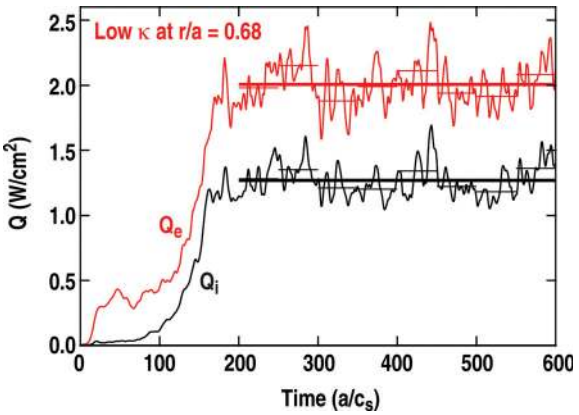

FIG. 5. (Color online) Time histories of box-averaged ion and electron energy fluxes for a GYRO simulation of the low κ discharge at $r/a = 0.72$. The mean values are plotted as the thick lines, while the average values over consecutive 50 a/c_s windows plotted as thinner lines. Estimating the statistical uncertainty of the mean fluxes as the standard deviation of the mean of the 50 a/c_s realizations yields $Q_i = 1.27 \pm 0.03$, $Q_e = 2.01 \pm 0.03$ W/cm^2.

Ideally, one would like to test these transport predictions against direct measurements of the corresponding particle, energy and momentum fluxes. Unfortunately, such measurements are not available in the core region of typical high power plasma discharges such as those considered here, due to the lack of localized radial velocity fluctuation measurements which could be correlated with density, temperature, or velocity fluctuations to calculate Q_i or Q_e. However, one can make an independent calculation of the expected fluxes via a power balance analysis. Starting with the relevant transport equation, e.g., the flux-surface averaged energy equation

$$\frac{3}{2}\frac{\partial \langle nT \rangle}{\partial t} + \frac{1}{V'}\frac{\partial}{\partial r}(V'Q) = \langle S \rangle, \tag{1}$$

where brackets denote a magnetic flux surface average, V' is the differential volume element, and S is the sum of any sources or sinks at a given radius, the steady state flux Q can be calculated as

$$Q = \frac{1}{V'}\int_0^r dx V' \langle S \rangle, \tag{2}$$

While both turbulent and neoclassical processes contribute to these fluxes, in practice the turbulent fluxes dominate for most plasmas (particularly L-mode discharges such as these) except for the ion heat transport near the magnetic axis. There exists a wide range of tools and codes for calculating these source terms, as well as sinks due to radiation and collisional processes, many of which have undergone their own verification and validation exercises. For this elongation

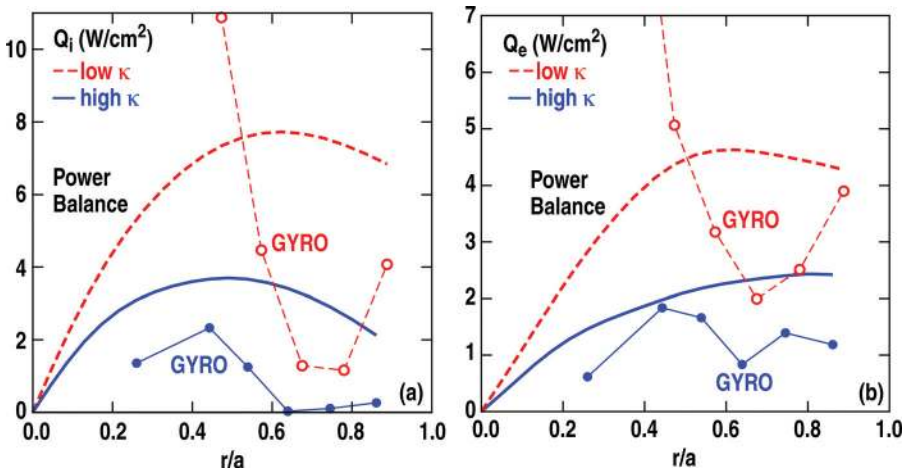

FIG. 6. (Color online) Comparisons of GYRO (•) predictions for (a) Q_i and (b) Q_e against ONETWO (−) power balance calculations, for both high and low κ discharges.

study, we have used the ONETWO code[33] to perform the power balance analysis, using the NFREYA module[34] to calculate the relevant source terms due to neutral beam injection. We also restrict consideration to only the energy fluxes Q_i and Q_e for the remainder of this paper, due to both space constraints and uncertainties in relevant source terms for the particle and momentum power balance analysis. A more complete investigation of all transport channels will be pursued in future work.

In Fig. 6, we show comparison of the GYRO-predicted magnetic flux-surface averaged ion and electron energy fluxes Q_i and Q_e against corresponding ONETWO power balance calculations. The dominant impression the comparisons provide is that while there is a global consistency of increased transport with reduced elongation in the simulation results, there are clear discrepancies between the GYRO and power balance results in both quantitative levels and, more importantly, trends with r/a for both plasma conditions. In the high κ case, the transport is systematically underpredicted at all radii, with a transition from ion mode turbulence at smaller r/a to electron mode dominant turbulence at larger r/a occurring around $r/a = 0.6$. The simulation at $r/a = 0.64$ should be given rather less weight than the other points because it does not resolve the full range of electron-transport relevant wavenumbers, as shown in Fig. 7. One could easily imagine a simulation that properly captured the full range of electron transport relevant scales (likely up to $k_\theta \rho_s = 6$–10 if not more) could lead to a doubling of the predicted electron transport, yielding a predicted Q_e at $r/a = 0.64$ more in line with the neighboring simulations. However, it is unlikely that this would increase the predicted Q_i, which can only occur at experimentally relevant levels below $k_\theta \rho_s \sim 1$, or perhaps 2 in the case of carbon ions. Carbon ions can carry significant transport at higher values of Z_{eff}, driving 20% of the total Q_i in some of the high κ results shown here.

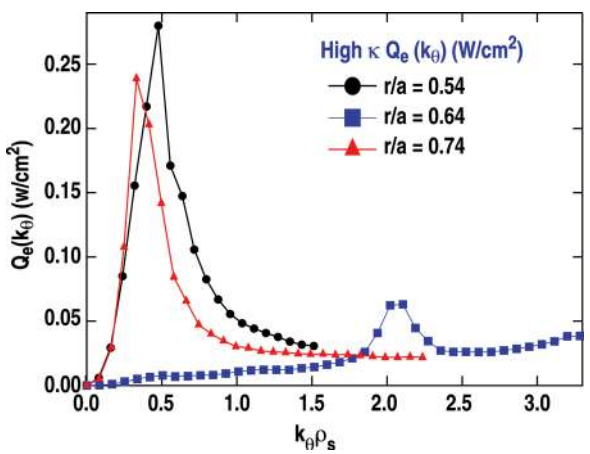

FIG. 7. (Color online) Comparisons of $Q_e(k_\theta)$ for GYRO simulations of the high κ discharge at $r/a = 0.54$ (•), 0.64 (■), and 0.74 (▲).

In contrast to the high κ results, the low κ GYRO simulations significantly overpredict the power balance results at small r/a (with GYRO predicting $Q_i = 51$ W/cm^2 and $Q_e = 17$ W/cm^2 at $r/a = 0.28$), but rapidly decrease with increasing r/a such that there is a systematic underprediction at larger r/a. There is a particularly interesting uptick in the simulations at $r/a \geq 0.8$, which is not observed in the high κ case or in other gyrokinetic modeling of similar high κ DIII-D discharges,[8,12] while GYRO simulations of Tore Supra Ohmic discharges[11] (which have low κ) report close agreement with power balance results even at larger r/a. Whether the now well-established underprediction of L-mode near-edge transport and turbulence by gyrokinetic models in many discharges has a shaping dependence is a topic deserving further investigation.

Given the strong radial variations in the local GYRO flux predictions of the low κ discharge, one might wonder about the suitability of the local approximation. To quantify the magnitude of nonlocal effects (spatial variations of dimensionless parameters such as κ, a/L_{Ti}, T_e/T_i, and magnetic shear), a pair of nonlocal simulations centered at $r/a = 0.28$ and 0.68 were performed; the results are shown in Fig. 8. While there is a clear reduction in the predicted transport at $r/a = 0.28$ in the nonlocal simulation relative to the local result, the nonlocal simulations remain a factor of 5–10 times higher than the power balance results and smoothly decrease with radius to essentially match the local results at $r/a = 0.47$. The large r/a nonlocal simulation shows some smaller quantitative differences with the local results but still exhibits a clear systematic underprediction of both ion and electron transport across the simulation domain. The difference between the local and global results is also quite consistent with previous ρ^* scaling studies, which

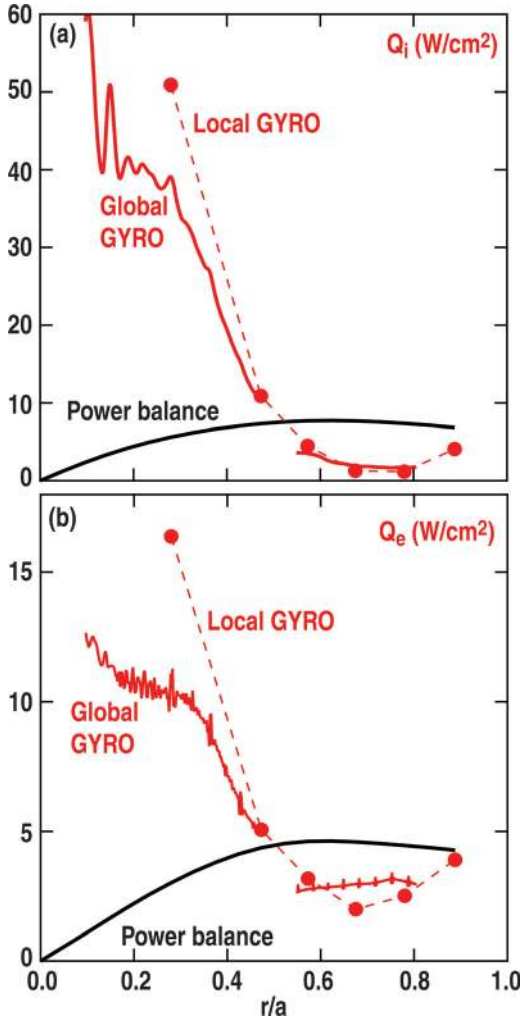

FIG. 8. (Color online) Comparisons of global and local GYRO predictions for (a) Q_i and (b) Q_e against ONETWO power balance results for low κ discharge 136693.

found global transport moderately lower than the corresponding local result when $1/\rho^* \sim 250$ (which it is at $r/a = 0.28$), but essentially the same for the $r/a = 0.68$ value of $1/\rho^* \sim 400$ (Ref. 35). Thus, we conclude that the source of the discrepancies between the gyrokinetic model and power balance results does not arise from use of the local approximation.

C. Comparison of GYRO-predicted fluctuation levels against experimental measurements

While the assessment of consistency (or lack thereof) between the gyrokinetic and power balance flux calculations presented in Sec. III B is a necessary first step in this validation study, it is insufficient in and of itself because it compares two modeled quantities, rather than model predictions against actual measurements. Moreover, it does not address whether the gyrokinetic model accurately describes the underlying physics of the turbulent fluctuations and their correlations that drive the transport. To address both these issues, we now turn to comparisons of model predictions to the measured density and electron temperature fluctuations shown in Fig. 3. In order for these comparisons to be quantitatively meaningful, it is essential to use synthetic diagnostics,[12,36,37] which account for differences between the measurements and the simulation output due to, e.g., finite spatiotemporal sensitivities in the actual diagnostics. To account for the fact that both the BES and CECE diagnostics integrate radiation from finite spatial volumes, the GYRO simulated electron density and temperature fluctuations are convolved with spatial transfer functions to generate arrays of time series from nearby locations, as is done in Holland *et al.*[12] These synthetic time series are then used to calculate statistically converged cross-spectra that are integrated over certain frequency bands (70–300 kHz for the BES diagnostic and 0–350 kHz for the CECE diagnostic), as is done in the experiment. The lower limit for the BES diagnostic is set by small oscillations in the neutral beam voltage, which can overwhelm the turbulence spectrum at low frequencies.

Comparisons of synthetic RMS BES and CECE amplitudes for both conditions are shown in Fig. 9. As in previous studies,[12] we observe a clear correlation between the level of agreement in the synthetic and measured fluctuation levels at a given radius and the agreement between gyrokinetic and power balance flux predictions at that location. The calculated high κ fluctuations systematically underpredict the measurements at almost all radii, with a similar trend in radius as the energy fluxes. The sole exception is the rather surprisingly good agreement in δT_e at $r/a = 0.86$, given the significant underprediction of Q_e at that location. Theoretically, one might have expected that the roughly factor of 2

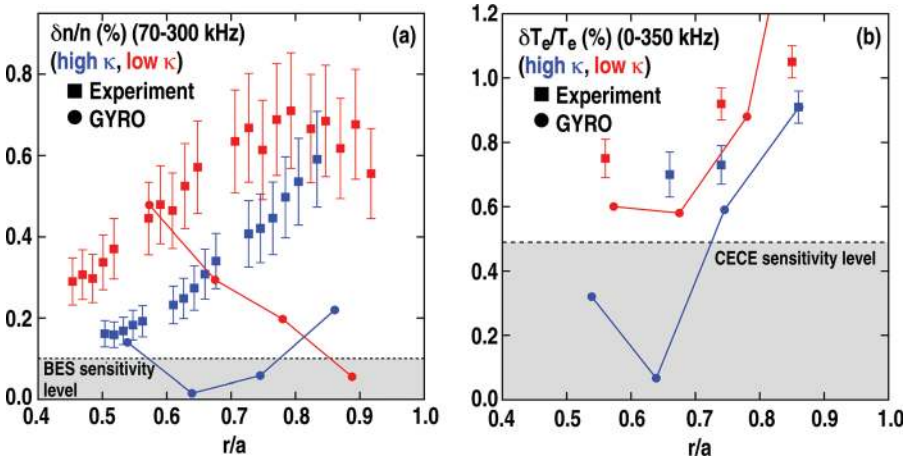

FIG. 9. (Color) Comparisons of GYRO (•) predictions of locally normalized (a) density and (b) electron temperature fluctuations against experimental measurements (■), for both the high and low κ discharges.

underprediction of the power balance results by GYRO would lead to between a factor of $\sqrt{2}$ to 2 underprediction in δT_e, depending on whether one assumed a scaling of Q_e with "fluctuation amplitude" squared (as was observed in Ref. 12) or a stronger linear scaling of Q_e with δT_e. However, either expectation assumes that the power balance results accurately represent the actual experimental transport, which may not be the case. Future work should test this assumption more closely, examining whether use of a more sophisticated neutral beam modeling package [such as NUBEAM (Ref. 38)] would yield significantly different predictions, and what impact inclusion of the turbulent energy exchange[39] would have on the predicted fluxes.

The low elongation synthetic fluctuations exhibit a fairly similar behavior relative to the corresponding energy fluxes as the high elongation predictions. In particular, the low κ synthetic δT_e fluctuation predictions increase with radius but underpredict the measured levels at most radii, except at $r/a = 0.89$ where the predicted RMS amplitude is 1.8% versus a 1.05% measured level. This radial trend is consistent with the gyrokinetic Q_e predictions that are increasing with r/a but still less than or almost equal to (at $r/a = 0.89$) the power balance results across the considered domain. The synthetic low κ density fluctuations also exhibit a similar decrease and underprediction of experimental data with increasing r/a as the energy fluxes but do not exhibit the uptick at large r/a the predicted fluxes do. This breaking in fluctuation trends can be understood by examination of the synthetic spectra, which indicate that most of the turbulent fluctuation power in the low κ discharge simulations (but not experiment) is below 70 kHz at large r/a, such that it is excluded from the synthetic density but not temperature fluctuation integrations. So while the predicted density fluctuations integrated only over the 70–300 kHz range do not show the uptick at the largest r/a the energy fluxes do, integrating the low κ density fluctuations over all frequencies does reproduce this trend; for instance, a synthetic BES level of 0.55% is predicted at $r/a = 0.88$ when integrated over all frequencies. Thus, the total predicted fluctuation amplitudes exhibit trends consistent with the flux predictions, but this correlation is broken for the density fluctuations by the details of the synthetic diagnostic calculation. This breaking should be viewed as a strength rather than a weakness of the comparison, because it tests not just the total predicted fluctuation amplitudes, but also the distribution of fluctuation power at different frequencies (i.e., it tests the predictions of the underlying shape of the fluctuation spectra) and highlights a deeper discrepancy between the model predictions and experimental measurements which might otherwise have been missed. Future work will explore agreement and disagreement in predicted and measured spectra in greater detail.

D. Uncertainty quantification for stiff transport models

An essential issue that must be addressed in any validation study is that of uncertainty quantification. While the use of long time averages of both the experimental data and nonlinearly saturated phases of the simulations minimizes the impact of the simple statistical uncertainties, the more subtle issues of systematic uncertainties and model sensitivities remains. In the case of turbulent transport, this issue manifests most clearly in terms of stiffness—the frequent observation that a small change in an equilibrium parameter (most commonly one of the driving temperature or density gradient scale lengths or the local equilibrium $\vec{E} \times \vec{B}$ shearing rate) can lead to a large change in the predicted level of transport and turbulence intensity. Often (particularly for simplified theoretical considerations of turbulence instabilities), there is a critical value of a single key driving gradient, such that below this value little transport is predicted, but above which the transport increases rapidly as this gradient is further increased above the critical value. Examples of this behavior include both the multicode CYCLONE benchmarking study of adiabatic electron ITG turbulence,[40] as well as experimental observations in both the ion[41,42] and electron[43] thermal channels. The possibility of stiff transport generally dominates the uncertainty of simulations like those discussed in this section, because the uncertainties in profile gradients (the model inputs) derived from experimentally measured quantities will always be larger than the uncertainties in the measured quantities themselves. The fact that these gradients are often derived not directly from the experimental data, but from smoothly varying fits to point measurements, only enhances the possibility of non-negligible uncertainties in the local gradient values.

While the idea of transport stiffness is easy to express qualitatively, it is more challenging to formulate a quantitative definition of stiffness robust enough to be useful for the full breadth of complicated transport phenomenon observed experimentally. This complication is particularly challenging in plasmas where multiple instabilities are present, each with their own dependencies and critical parameters. In this paper, we use the approach of Waltz *et al.*,[44] and define the stiffness S of a particular flux Q to an input parameter z as

$$S = \frac{z}{Q}\left(\frac{dQ}{dz}\right), \tag{3}$$

with all other parameters held fixed. Using this definition, a simple linear flux-gradient relationship (such as the neoclassical ion heat flux) would be said to have $S = 1$. On the other hand, a doubling of the predicted heat flux (a 100% increase) in response to a 10% increase in an input gradient scale length would yield $S = 10$. Thus, the qualitative idea of stiffness described above can be expressed quantitatively as a value of $S \gg 1$. This definition is suitably general to describe a wide variety of observed phenomena (such as the stiffness of the electron energy flux Q_e to a change in a/L_{Ti} in ITG turbulence, or with respect to the magnetic safety factor q), but it specifically does not reference the proximity in parameter space to a critical gradient or other parameter, as such critical parameters are not always easily or simply identified in realistic conditions.

There are several ways to address the issue of systematic uncertainties due to model stiffness, none of which has been routinely implemented or accepted as sufficient in and of itself within the magnetic fusion community at this time. The most basic and commonly used approach is essentially

TABLE I. GYRO sensitivity study for the high elongation $r/a = 0.54$ case. For each input parameter variation, both the absolute magnitude of the fluxes and their corresponding stiffness $S = d\ln Q_{i,e}/d\ln z$ are listed.

High κ ($r/a = 0.54$)	Q_i (W/cm^2)	Q_e (W/cm^2)
Power balance	3.6	2.2
GYRO (base)	1.25 ± 0.02	1.67±0.03
GYRO (+10% a/L_{Ti})	2.67±0.08 ($S = 11.4$)	2.92±0.07 ($S = 7.5$)
GYRO (+10% a/L_{Te})	1.33±0.04 ($S = 0.6$)	2.11±0.05 ($S = 2.6$)
GYRO (+10% a/L_{ne})	1.36±0.04 ($S = 0.9$)	1.76±0.05 ($S = 0.5$)
GYRO (+10% $\gamma_{E\times B}$)	0.90±0.03 ($S = -2.8$)	1.22±0.03 ($S = -2.7$)

TABLE III. GYRO sensitivity study for the high elongation $r/a = 0.75$ case. For each input parameter variation, both the absolute magnitude of the fluxes and their corresponding stiffness $S = d\ln Q_{i,e}/d\ln z$ are listed.

High κ ($r/a = 0.75$)	Q_i (W/cm^2)	Q_e (W/cm^2)
Power balance	2.9	2.4
GYRO (base)	0.102 ± 0.002	1.39 ± 0.03
GYRO (+10% a/L_{Ti})	0.075 ± 0.002 ($S = -2.6$)	1.04 ± 0.03 ($S = -2.5$)
GYRO (+10% a/L_{Te})	0.123 ± 0.002 ($S = 2.1$)	1.79 ± 0.03 ($S = 2.9$)
GYRO (+10% a/L_{ne})	0.106 ± 0.001 ($S = 0.4$)	1.22 ± 0.02 ($S = -1.2$)
GYRO (+10% $\gamma_{E\times B}$)	0.094 ± 0.001 ($S = -0.78$)	1.28 ± 0.01 ($S = -0.79$)

a series of sensitivity tests, in which the various model inputs are systematically varied one-by-one and changes in the predicted transport and turbulence characteristics quantified. The results of this approach, as applied to the model predictions at both $r/a = 0.55$ and 0.75, are shown in Tables I–IV. At each location, four key driving gradients (a/L_{Ti}, a/L_{Te}, a/L_{ne}, and $\gamma_{E\times B}$) were individually increased by 10%, and the response of the transport levels quantified in both absolute magnitude and stiffness S. At $r/a \sim 0.55$ (Tables I and II), we see that both cases exhibit a response consistent with ITG-dominated turbulence, with the strongest responses in both Q_i and Q_e coming from changes in a/L_{Ti}. However, examination of Tables I and II also clearly shows that Q_i and Q_e have different amounts of stiffness with respect to changes in a/L_{Ti} and a/L_{Te}, such that a simple statement regarding overall transport stiffness could be misleading. Examination of the responses at $r/a \sim 0.75$ (Tables III and IV) illustrates another challenge for quantifying stiffness in real plasmas, which is that stiffness to different parameters can change significantly at different locations in the plasma. For instance, the turbulence at $r/a = 0.78$ in the low κ discharge remains ITG-dominated, with the strongest response to a/L_{Ti}, but now exhibits a significantly reduced sensitivity to γ_{ExB}. In the case of the high κ discharge, however, the turbulence at $r/a = 0.75$ is now TEM-dominated, and the sensitivities to the various gradients have shifted accordingly.

A second approach to understand the stiffness and sensitivity of the turbulence is to recast the comparison in terms of predicted fluxes as a function of driving gradient, analogous to the approach used in the experimental studies.[41–43] While this approach is also limited in general by the complexities of multimode turbulence described above, it can in principle still provide a useful measure for testing model predictions against experiment and making contact with past work. Comparisons of power balance and model predictions of Q_i as a function of a/L_{Ti} and Q_e versus a/L_{Te} are shown in Fig. 10. These data are the same as in Fig. 6, only now we use the temperature scale lengths at each radius as the independent variable, rather than the radius itself. The energy fluxes have also been normalized to the gyroBohm value $Q_{gB} = n_e T_e c_s (\rho^*)^2$. Using this definition, it is easy to recast the simple dimension flux-gradient relationship $Q = -n\chi\nabla T$ into a dimensionless form $Q/Q_{gB} = (\chi/\chi_{gB})(a/L_T)$, where $\chi_{gB} = \rho_s^2 c_s/a$. Thus, this normalization both removes the expected "zeroth order" radial dependencies on the equilibrium temperature, density, and magnetic field (through ρ^*) and helps make contact with the theoretical framework which is generally cast in terms of the gyroBohm scalings and normalizations. However, since this comparison does not hold dimensionless parameters fixed as a/L_T varies [the plots are of $Q(r)/Q_{gB}(r)$ vs $a/L_T(r)$], it is not a true comparison of stiffness as defined in this paper. Nonetheless, it is interesting to note the clear differences between the fidelity of the ion and electron transport predictions to the power balance results in this formulation. While the electron transport is systematically underpredicted by up to a factor of 2, the gyrokinetic predictions do exhibit a qualitatively similar dependence on a/L_{Te} as the power balance calculations. In contrast, there are significant differences observed at both the quantitative and qualitative level between the power balance calculations and gyrokinetic predictions for the ion transport. Thus in these plasmas, a challenge for future studies is to understand why predictions of the ion thermal transport exhibit significantly worse agreement with power balance calculations than the electron thermal transport.

TABLE II. GYRO sensitivity study for the low elongation $r/a = 0.55$ case. For each input parameter variation, both the absolute magnitude of the fluxes and their corresponding stiffness $S = d\ln Q_{i,e}/d\ln z$ are listed.

Low κ ($r/a = 0.55$)	Q_i (W/cm^2)	Q_e (W/cm^2)
Power balance	7.7	4.6
GYRO (base)	4.50 ± 0.05	3.16 ± 0.04
GYRO (+10% a/L_{Ti})	6.1 ± 0.2 ($S = 3.6$)	3.95 ± 0.08 ($S = 2.5$)
GYRO (+10% a/L_{Te})	4.31 ± 0.08 ($S = -0.4$)	3.47 ± 0.06 ($S = 1.0$)
GYRO (+10% a/L_{ne})	4.65 ± 0.09 ($S = 0.3$)	3.29 ± 0.05 ($S = 0.4$)
GYRO (+10% $\gamma_{E\times B}$)	3.9 ± 0.1 ($S = -1.3$)	2.72 ± 0.09 ($S = -1.4$)

TABLE IV. GYRO sensitivity study for the low elongation $r/a = 0.78$ case. For each input parameter variation, both the absolute magnitude of the fluxes and their corresponding stiffness $S = d\ln Q_{i,e}/d\ln z$ are listed.

Low κ ($r/a = 0.78$)	Q_i (W/cm^2)	Q_e (W/cm^2)
Power balance	7.4	4.5
GYRO (base)	1.16 ± 0.01	2.50 ± 0.03
GYRO (+10% a/L_{Ti})	1.80 ± 0.03 ($S = 5.5$)	2.80 ± 0.03 ($S = 1.2$)
GYRO (+10% a/L_{Te})	0.92 ± 0.01 ($S = -2.1$)	2.75 ± 0.03 ($S = 1.0$)
GYRO (+10% a/L_{ne})	1.15 ± 0.02 ($S = -0.1$)	2.50 ± 0.03 ($S = 0.0$)
GYRO (+10% $\gamma_{E\times B}$)	1.11 ± 0.01 ($S = -0.4$)	2.43 ± 0.02 ($S = -0.3$)

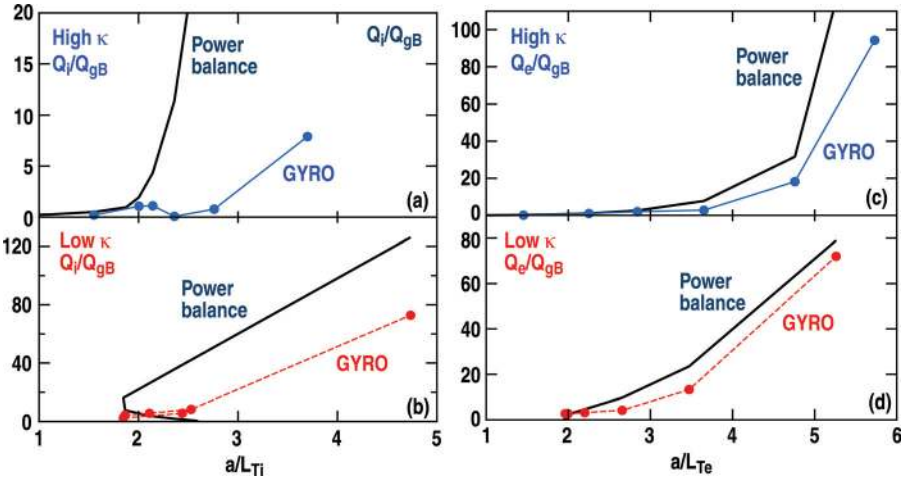

FIG. 10. (Color online) Comparisons of gyro-Bohm normalized energy fluxes as function of driving gradient. (a), (b) Q_i/Q_{gB} as a function of a/L_{Ti} is plotted for the (a) high κ and (b) low κ discharges. (c), (d) Q_e/Q_{gB} as a function of a/L_{Te} for the (c) high κ and (d) low κ discharges. Note that fluxes Q_i and Q_e, the gyro-Bohm factor Q_{gB}, and the gradient scale lengths a/L_{Ti} and a/L_{Te} are all functions of r/a, such that these comparisons are not pure tests of local transport stiffness as other dimensionless parameters are also varying.

IV. ASSESSING SYSTEMATIC UNCERTAINTIES VIA USE OF TGLF TRANSPORT SOLUTION PROFILES

The results of Sec. III exhibit clear and statistically significant differences between power balance flux calculations, experimentally measured RMS fluctuation amplitudes, and the corresponding gyrokinetic predictions, when the equilibrium profiles are given as inputs to GYRO. In addition to the approaches discussed in Sec. III D (sensitivity analysis and plots of normalized flux versus driving gradient), a third approach to addressing the issue of stiff transport and gradient uncertainties is through the calculation of transport solution profiles. The flux comparisons presented in Sec. III B can be summarized as

$$Q_{\mathrm{GYRO}}\left(n^{\mathrm{exp}},T^{\mathrm{exp}},E_{\mathrm{r}}^{\mathrm{exp}}\right)\neq\frac{1}{V'}\int_0^{\mathrm{r}}dxV'\left\{S_{\mathrm{ext}}+S_{\mathrm{exch}}\left(n^{\mathrm{exp}},T^{\mathrm{exp}}\right)\right\} \tag{4}$$

That is, using the experimental profiles, the GYRO-predicted energy fluxes do not equal the volume integrals of the external sources S_{ext} (assumed to be independent of, or at least highly insensitive to, the equilibrium profiles) and collisional energy exchange term $S_{\mathrm{exch}}=n\left(T_{\mathrm{i}}-T_{\mathrm{e}}\right)/\tau_{\mathrm{ei}}$. However, assuming that the transport is in fact sufficiently stiff, one should be able to identify a set of transport solution profiles n^{TS}, T^{TS}, and $E_{\mathrm{r}}^{\mathrm{TS}}$, which are very similar to the experimental profiles but satisfy the Eq. (3),

$$Q_{\mathrm{GYRO}}\left(n^{\mathrm{TS}},T^{\mathrm{TS}},E_{\mathrm{r}}^{\mathrm{TS}}\right)=\frac{1}{V'}\int_0^{\mathrm{r}}dxV'\left\{S_{\mathrm{ext}}+S_{\mathrm{exch}}\left(n^{\mathrm{TS}},T^{\mathrm{TS}}\right)\right\} \tag{5}$$

More generally, one can calculate the transport solution profiles and assess how good a fit they are to the underlying point profile measurements, relative to the original "experimental" fits, regardless of the actual stiffness exhibited by the model. Good agreement between the transport solution profiles and experimental measurements would indicate that much of the observed disagreement could be attributed to systematic errors in the gradients of the experimental fits being magnified by the inherent transport stiffness. Conversely, poor agreement between the transport solution profiles and measurements would indicate that the differences between model and experiment could not be reconciled within the context of stiff transport and uncertainties in the model inputs.

This approach offers several useful advantages for testing stiff models over the simple sensitivity tests described in Sec. III D. First, by recasting the problem in terms of global profiles predicted for a specified flux profile, the issue of large uncertainties in the input gradients can be sidestepped. Second, it allows a self-consistent variation of multiple parameters to yield a more systematic approach to stiffness in the presence of complex, multimode turbulence. However, this approach is not entirely satisfactory for testing turbulence models, particularly local ones, as the test becomes inherently nonlocal—the performance of the model at other radii impacts the performance of the model at the location of interest. Thus, the transport solution approach should be viewed as complementary to tests of model sensitivity and uncertainty, such as those discussed in Sec. III D, rather than superseding them.

The primary challenge in direct calculation of transport solution profiles lies with the computational cost, which can easily be an order of magnitude larger than simply evaluating the transport at multiple radii for a fixed profile set. Nonetheless, algorithms to perform such calculations for both local[45] and global[46] GYRO simulations have been implemented within the TGYRO transport code.[45] An additional advantage of the TGYRO code is that it can also calculate transport solution profiles using the quasilinear TGLF model.[23,24] The TGLF model combines linear phase relations calculated from a 15-moment set of fluid equations with a nonlinear saturation rule fit against a large database of nonlinear GYRO runs to make rapid predictions of turbulent transport (requiring minutes or less on a desktop machine, relative to thousands of CPU-hours for fully converged nonlinear GYRO simulations). Furthermore, both the linear mode relations and transport predictions made by TGLF have been verified, with good agreement, against corresponding GYRO predictions.

Taking advantage of this expected correspondence between TGLF and GYRO predictions, TGLF was used as a proxy for GYRO in the TGYRO code to calculate transport solution temperature profiles (with density and radial electric

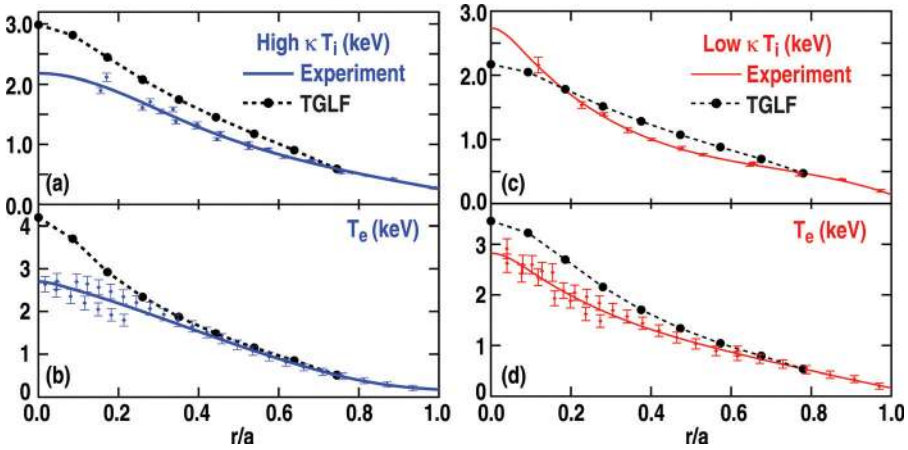

FIG. 11. (Color online) Comparisons of TGLF-predicted transport solution profiles (•) against experimental profiles [spline fits to measured points (◆)] for the high (solid) and low (dashed) κ discharges.

field profiles held fixed at the experimental fits); the analysis presented in Sec. III is then repeated using these transport solution profiles as inputs to GYRO to predict the energy fluxes and fluctuation levels. We choose to hold the density profile fixed because there was no readily available verified model for calculating the particle source term due to wall-recycling neutrals during this analysis. The rotation profile (and thus E_r profile) is held fixed because the TGLF momentum transport predictions had not been fully verified against GYRO at the time this analysis was conducted. Although TGLF energy (and particle) flux predictions have been verified against GYRO over a wide range of parameters, exact agreement between the two should not be expected for any given set of inputs. Rather, it is expected that TGLF will be able to provide a reasonably accurate measure of the response of the GYRO simulations to changes in the input parameters, such that improved (but not perfect) agreement in the energy fluxes will be found using the TGLF-predicted transport solution.

The TGLF transport solutions are shown in Fig. 11, along with the experimental measurements and fits used in Sec. III. The transport solutions are calculated by specifying a fixed or pivot point in the range of $r/a = 0.75$–0.78 and then integrating inward. The choice of pivot locations is determined by the significant underprediction (particularly of the high κ case) at larger radii, which prevents TGYRO from obtaining a converged solution at larger radii.

The results shown in Fig. 10 are quite consistent with what would be expected from the differences in the GYRO and power balance fluxes shown in Fig. 6. The strong underprediction of the high κ Q_i at all radii leads to a transport solution T_i profile with equal or steeper gradients across the considered domain, whereas the much closer agreement in Q_e leads to significantly smaller changes for $r/a > 0.2$. These results are consistent with the sensitivity studies shown in Tables I and III, which found that Q_i and Q_e were significantly stiffer with respect to a/L_{Ti} but not a/L_{Te} at $r/a = 0.54$, but not stiff with respect to a/L_{Ti} at $r/a = 0.75$ (the transport in fact decreased with a small increase in a/L_{Ti}). It is also worth noting the separation of high- and low-field ECE channels evident inside $r/= 0.2$ for the high κ T_e plot. This separation is generally evidence of an error in the calculation of the magnetic axis and represents another typical systematic error (errors in the magnetic equilibrium) that must be considered in validation studies. It is interesting to note that splitting of high- and low-field ECE channels corresponds to the beginning of a significant divergence in the transport solution T_e profile from the measurements. Whether this near-axis discrepancy persists when an equilibrium with improved magnetic axis location is used will be addressed in future work. Similarly, the low κ transport solution profiles (particularly the T_i profile) can easily be understood in terms of the observed differences shown in Fig. 6 and the sensitivity tests shown in Tables II and IV in a manner similar to the high κ results.

The GYRO-predicted energy fluxes and fluctuation levels using the high κ transport solution are shown in Fig. 12.

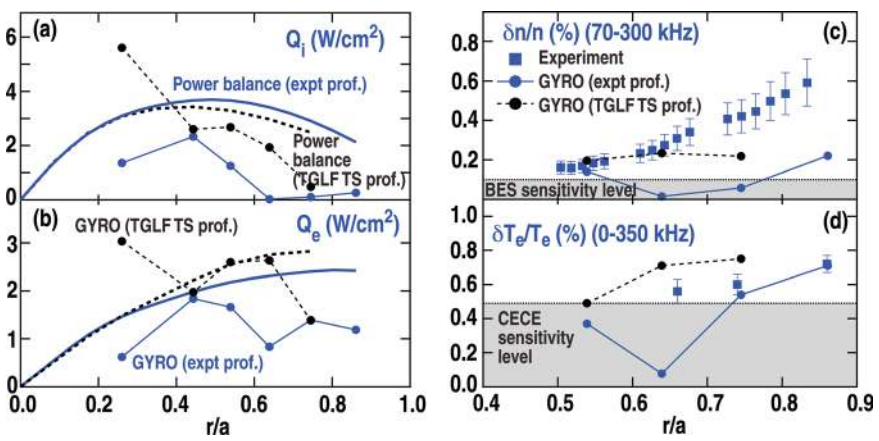

FIG. 12. (Color) Comparisons of GYRO-predicted (a) Q_i, (b) Q_e, (c) $\delta n/n$, and (d) $\delta T_e/T_e$ (d) for the high κ discharge (136674) using the experimental (•) and TGLF-predicted transport solution profiles (•) as inputs. Power balance calculations of Q_i and Q_e using the experimental profiles are plotted as solid curves in (a) and (b), and the calculations based upon the TGLF-predicted profiles are plotted as dashed lines.

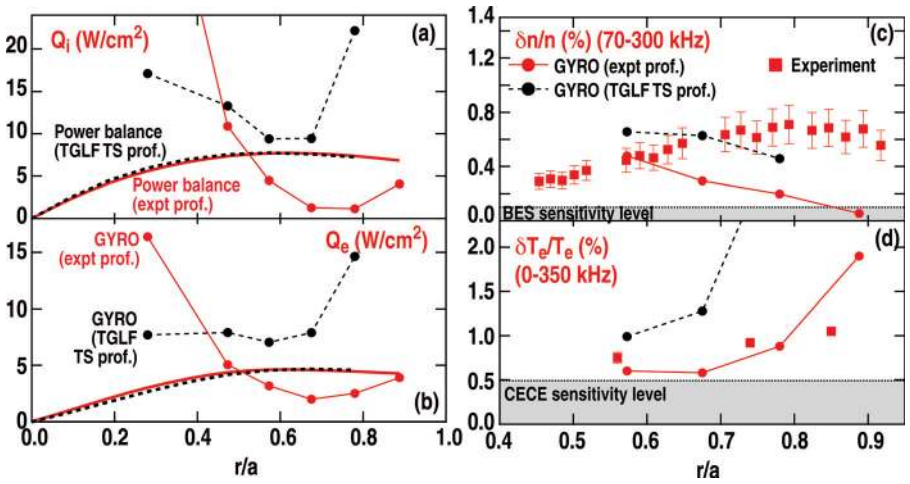

FIG. 13. (Color) Comparisons of GYRO-predicted (a) Q_i, (b) Q_e, (c) $\delta n/n$, and (d) $\delta T_e/T_e$ for the low κ discharge (136693) using the experimental (•) and TGLF-predicted transport solution profiles (•) as inputs. Power balance calculations of Q_i and Q_e using the experimental profiles are plotted as solid curves in (a) and (b), and the calculations based upon the TGLF-predicted profiles are plotted as dashed lines.

Note that the relevant comparison is between the dashed black curves (which are equal to the TGLF-predicted transport solution fluxes and differ from the initial power balance calculation due to the self-consistent changes to the exchange) and the filled black circles (the GYRO predictions which use the TGLF-predicted transport solutions as inputs). As expected, a significantly closer agreement between GYRO and the transport solution power balance results is seen at most radii. Also as expected, the agreement and responses are not exact, with the GYRO underpredictions at $r/a = 0.26$ becoming overpredictions when using the TGLF profile predictions and the underprediction of Q_i persisting at large r/a, albeit at a reduced level. Somewhat more surprising is that only very small increases in the GYRO-predicted transport are observed at $r/a = 0.44$ and 0.74, despite changes in temperatures and gradients at these locations; the relatively modest change in Q_i at $r/a = 0.74$ despite the strong increase in a/L_{Ti} is quite striking, although consistent with sensitivity analysis in Table III. This observation further supports the conclusion drawn from the interpretation of the transport solution profiles that strong stiffness in turbulent transport models is not a simple and universal phenomenon, but rather has complex dependencies that are not fully understood yet. Developing a better understanding of what determines the transport stiffness in experiments and simulations is essential for improving the confidence in predicting the performance of future devices such as ITER.

Figure 12 also shows that the magnitude of the predicted density and temperature fluctuations increases quite significantly when the TGLF transport solution profiles are used as the inputs to GYRO. Most notable is the increase in the predicted value of the temperature fluctuations, which systematically overpredict the measured levels when the TGLF transport solution profiles are input to GYRO. One possible source for some of the observed discrepancy between the observed and expected relationships between predicted fluctuation intensities and turbulent fluxes is that significant net particle pinches are predicted for both the experimental and TGLF transport solutions (which only vary the T_i and T_e profiles) over the range $0.44 < r/a < 0.74$. At $r/a = 0.74$, for instance, the magnitude of the GYRO-predicted (inward) convective electron energy flux $Q_{e,conv} = (3/2)T_e\Gamma_e$ (where Γ_e is the electron particle flux) is essentially zero (0.3% of the total Q_e) for the experimental profiles, but increases significantly to have a magnitude of 20% of the total Q_e at $r/a = 0.74$ when using the TGLF transport solution profiles. Developing a better understanding of the interplay between electron density and temperature gradients, the corresponding particle and energy fluxes and the underlying density and temperature fluctuations are yet another area that should receive more attention in future work.

The GYRO predictions using the low κ TGLF transport solution profiles as inputs are shown in Fig. 13. The changes in the GYRO predicted energy fluxes shown in Figs. 13(a) and 12(b) indicate an almost inverse sensitivity relative to the high κ discharge. At $r/a = 0.28$, the GYRO-predicted transport is reduced but still remains significantly higher than the power balance calculation, whereas the underprediction at $r/a = 0.26$ in the high κ case became an equally strong overprediction. Conversely, whereas only moderate increases in the predicted transport were observed at larger r/a in the high κ case, a strong increase in predicted transport is observed for the low κ discharge, such that Q_i and Q_e are over predicted by GYRO with the TGLF transport solution profiles as inputs across the entire plasma domain. As in the high κ case and consistent with the observed increased in predicted transport, we observe an increase in the predicted fluctuation levels at all radii considered, with $\delta T_e/T_e$ over predicted at all radii (reaching a value of 3.3% at $r/a = 0.78$). Interestingly, the predicted $\delta n/n$ profile maintains its strong decreasing trend with radius, despite the fact that that trend is eliminated from the predicted energy fluxes at the corresponding radii. These results are due to the bulk of the fluctuation power remaining below 70 kHz at large r/a, as was discussed in Sec. III.

V. COMPARISON OF GYRO PREDICTIONS TO A QUIESCENT H-MODE ELECTRON POWER SCAN

While most validation studies of nonlinear turbulence models (such as the one described above) have focused upon Ohmic or L-mode conditions that generally offer robust turbulence that can be (relatively) easily measured and quantified, it is important to examine the fidelity of the models in other

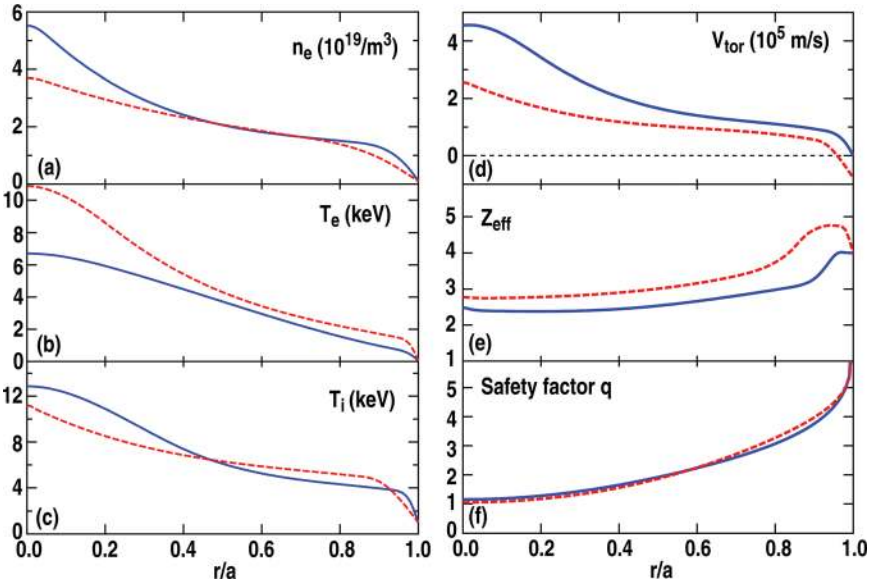

FIG. 14. (Color online) Equilibrium profiles for discharges 141397 (NBI heating only) (solid) and 141407 (NBI and ECH heating) (dashed), averaged from 4100 to 4150 ms: (a) electron density n_e, (b) electron temperature T_e, (c) ion temperature T_i, (d) torodial velocity V_{tor}, (e) $Z_{eff} = \sum_i Z_i^2 n_i \Big/ \sum_i Z_i n_i$, and (f) safety factor q.

operating regimes as well. In particular, assessing the fidelity of gyrokinetic predictions in high confinement (H-mode) plasmas is of significant interest as this operating regime is envisioned for future burning plasma and reactor devices. Toward this end, a H-mode validation experiment was performed on the DIII-D experiment to assess the ability of GYRO and other gyrokinetic-based models to predict the turbulence and transport levels in this confinement regime. The plasmas considered were so-called "quiescent" H-modes (QH-modes),[25,26] which were chosen because they do not exhibit the sawteeth or edge localized modes found in many other H-modes, but instead rely upon a highly localized edge mode (the edge harmonic oscillation, localized to $r/a > 0.8$–0.9) to maintain the equilibrium profiles in a true steady state. The experiment was designed to first obtain robust profile and fluctuation measurements in a baseline condition in which three neutral beam sources [providing a total of 6.9 MW of neutral beam injected (NBI) power] were injected in the counter-current direction. Measurements from a second steady-state condition, in which an additional 2.8 MW of ECH was injected with a resonance location near $r/a = 0.2$ (for a total of 9.7 MW of injected power), were then obtained to quantify the responses of the turbulence and transport to different applied heating mixes. The resultant profiles are shown in Fig. 14, showing that the application of ECH leads to clear changes in all of the profiles, particularly at small r/a.

As a first step in assessing model fidelity for these conditions, local GYRO runs were performed at $r/a = 0.6$ for each condition. Examination of the linear growth rates yielded a very similar story as for the L-mode study discussed above, namely that kinetic electrons and impurity physics had strong impacts on stability, while finite electromagnetic effects had only a small effect. The nonlinear simulations were thus performed using a very similar setup and resolution to the L-mode studies. The somewhat surprising results are given in Table V, which shows that the local gyrokinetic model used in these simulations over predicts the power balance Q_i calculation by a factor of 10 and Q_e by a factor of 25–70. The GYRO simulations also predict midplane $\delta n_e/n_e$ =2%–3% and $\delta T_e/T_e$ = 5%–6%, both of which are an order of magnitude larger than the corresponding measured values. The results of a sensitivity analysis that varied the driving scale lengths by 20% are also included within Table V. For any variation, the gyrokinetic predictions remained well above the power balance results, suggesting that stiffness or model sensitivity alone in the results cannot account for this difference. For instance, a 20% reduction of a/L_{Te} in the low T_e case had reduced Q_e by 30% (from 119 to 86 W/cm^2, corresponding to a stiffness $S = 1.4$), with virtually no effect on Q_i, and still well above the power balance value of 1.8 W/cm^2). Using the definition of stiffness given in Eq. (3), none of the responses would be

TABLE V. Comparisons of GYRO-predicted and ONETWO power balance calculations of Q_i and Q_e (which use the NUBEAM (Ref. 34) module to model the neutral beam physics) at $r/a = 0.6$, for both the low T_e NBI-only heating case (141397) and high T_e NBI + ECH heating case (141407). For each gradient variation, the corresponding stiffness is given following the definition of Eq. (3).

Q (W/cm^2)	Q_i (Low T_e)	Q_i (High T_e)	Q_e (Low T_e)	Q_e (High T_e)
Power balance	8.6	6.8	1.8	9.3
GYRO (base)	87.0 ± 1.0	78.0 ± 2.0	120.0 ± 1.0	209.0 ± 4.0
GYRO (-20% a/L_{Ti})	63.0 ± 1.0 ($S = 1.4$)	72.0 ± 5.0 ($S = 0.4$)	113.0 ± 1.0 ($S = 0.3$)	224.0 ± 12.0 ($S = -0.3$)
GYRO (-20% a/L_{Te})	82.0 ± 3.0 ($S = 0.3$)	68.0 ± 4.0 ($S = 0.9$)	80.0 ± 3.0 ($S = 1.7$)	148.0 ± 7.0 ($S = 1.4$)
GYRO (-20% a/L_{ne})	59.0 ± 2.0 ($S = 1.6$)	47.0 ± 1.0 ($S = 2.0$)	102.0 ± 2.0 ($S = 0.8$)	184.0 ± 3.0 ($S = 0.6$)
GYRO ($+20\%$ $\gamma_{E\times B}$)	86.0 ± 3.0 ($S = 0.0$)	76.0 ± 4.0 ($S = 0.0$)	113.0 ± 3.0 ($S = -0.3$)	211.0 ± 9.0 ($S = 0.0$)

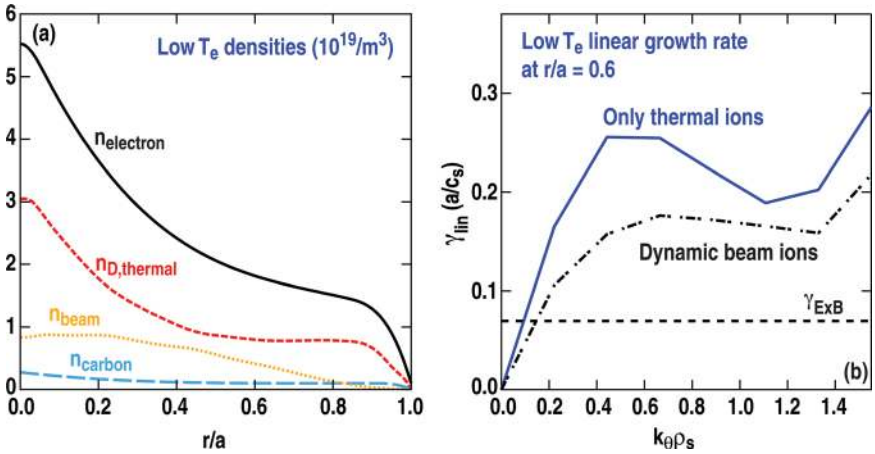

FIG. 15. (Color online) (a) Density profiles for various species: electrons (solid), thermal deuterium (dashed), "fast" deuterium ions from beam injection (dotted), and thermal carbon ions (long dashed) (for DIII-D discharge 141397 4125 ms. (b) Comparison of linear growth rates at $r/a = 0.6$ without (solid) and with (dot-dash-dot) dynamic fast beam ions included for 141397.

labeled to have $S > 2$, such that one cannot easily reconcile the discrepancies between the power balance and gyrokinetic flux predictions within plausible uncertainties due to stiffness.

There are several possibilities for the source of this large overprediction of turbulence levels. First, T_e is large enough that the standard radial box size of 90–100 ρ_s used in these simulations corresponds to roughly 40% of the plasma volume, bounding $0.4 < r/a < 0.8$. Thus, it is quite possible that inclusion of nonlocal effects could lead to a reduction in the predicted transport, in a similar fashion to the inner global simulation of the low κ discharge shown in Fig. 8. Given that the value of ρ^* at $r/a = 0.6$ in these discharges is quite close to the value of ρ^* at $r/a = 0.28$ in the low κ discharge are (4.0×10^{-3} and 4.3×10^{-3}, respectively), a similar proportional reduction in transport could be expected in these QH-mode predictions. Such a reduction alone would not be sufficient to eliminate the difference between the gyrokinetic and the power balance results, but it is interesting to note that the effect appears to be stronger for Q_e than Q_i, leading to a larger reduction of the larger discrepancy in Q_e.

A second likely source is in the treatment (or lack thereof) of fast ions in the simulations. In the simulation results listed in Table I, and as is done in virtually all published gyrokinetic turbulence modeling to date, the unthermalized fast ions present in the plasma due to neutral beam injection are not treated self-consistently, but rather "lumped in" to the thermal deuterium population. However, as seen in Fig. 15(a), these fast ions constitute a non-negligible fraction of the overall density (being roughly ~25% of the electron density at $r/a = 0.6$ in the NBI-only low T_e case, with similar levels in the high T_e case). A simple attempt to model these ions in a more realistic fashion can be made by treating them as an additional independent ion species, fluctuating about a background Maxwellian with a high temperature based on the modeled beam pressure (roughly 30–35 keV for these plasmas). While the assumption of a Maxwellian background is likely not a very good one, using it rather than incorporating, e.g., a slowing-down distribution may not matter much for drift-wave stability and turbulence calculations, as the fast ions will be, to leading order, adiabatic on ρ_s scales due to their relatively larger gyroradius (in the same way the thermal ions are adiabatic on electron gyroradius scales).[47] Using this assumption as a starting point, a significant reduction in linear growth rates is observed, as shown in Fig. 15(b). It should also be noted that these QH-mode discharges have rather low density (2–3 times smaller line averaged values) relative to "generic" H-modes and that this combination of low density plus strong neutral beam heating is what leads to the rather high fast ion fraction. We note that the NUBEAM code, rather than NFREYA, was used in these power balance calculations in order to properly account for the higher fast ion fraction and dynamics such as prompt losses that are not as significant in the L-mode plasmas. GYRO simulations of higher density H-modes, which did not include dynamic fast ions on both DIII-D[46] and Alcator C-mod,[14] exhibited significantly better agreement with power balance transport calculations and fluctuation measurements, further supporting this hypothesis. Perhaps the most direct way to asses the issue in future work will be to test the model against higher density QH-mode discharges, where careful optimization of the plasma boundary shape can yield line-average densities two to three times higher than in the discharges considered here (e.g., close to "conventional" H-mode levels).[48]

VI. FUTURE DIRECTIONS

While the validation of transport models remains a challenging and resource-intensive task, significant progress in our ability to test the models and their sensitivities against experiment is being made. For the L-mode plasmas discussed in this paper, there are clear differences observed between experimental measurements, power balance flux calculations, and model predictions when only the experimental profile fits are input to the model. It is possible that stiffness in the model predictions can account for some of these differences, but likely cannot explain all of them (notably the systematic underprediction of ion thermal transport in the high κ discharge). Future validation studies should further investigate the stiffness and sensitivities of the gyrokinetic model in these plasmas by utilizing self-consistently calculated transport solution profiles. A significant challenge for these future studies will be developing metrics for quantifying the tradeoff between discrepancies in fluxes in fixed-profile simulations and discrepancies between transport solution profiles and experimental measurements. That is, how

should the differences between gyrokinetic and power balance flux calculations as well as transport solution profiles and experimental profile measurements be quantified to best assess the relative fidelity of the fixed-profile and transport solution approaches? The results presented in this paper also emphasize the need to consider all transport channels, particularly the particle flux, in order to obtain not just fluxes but predicted fluctuation levels in better agreement with experiment. Future modeling of low density QH-mode plasmas will almost certainly need to include a better representation of fast ion physics and likely nonlocal effects as well; whether this issue persists at higher densities where the fast ion fraction will be significantly smaller should be assessed. Once these effects have been quantified, the underlying stiffness of the model predictions will need to be assessed as well. The implications of different fast ion equilibrium distributions should also be considered.

Beyond these additional gyrokinetic modeling activities, there are several issues related to the experimental measurements and their analysis which should be pursued. Foremost is quantifying the sensitivity of the gyrokinetic predictions to uncertainties and errors in the underlying magnetic equilibria. Fully assessing the fidelity of particle transport in either the fixed-profile or transport solution comparison modes will require a robust verified and validated model of the particle sources, particularly of the penetration of wall-recycling neutrals into the plasma core. Finally, going beyond comparisons of predicted and measured RMS fluctuation levels to more detailed comparisons of spectra and correlation lengths, and other fluctuations of interest (particularly zonal flows and geodesic acoustic modes[49]), as well as measures of coupling such as crossphases[15] and bispectral quantities[50] would add significantly to future studies.

ACKNOWLEDGMENTS

This work was supported by the US Department of Energy under DE-FG02-07ER54917, DE-FG02-06ER54871, DE-FG02-08ER54984, DE-FC02-04ER54309, DE-FG02-95ER54309, DE-FG02-89ER53296, DE-FG02-08ER54999, and DE-FC02-99E4512. This research was performed in collaboration with the Center for Simulations of Plasma Microturbulence and used resources of the National Center for Computational Sciences at Oak Ridge National Laboratory, which is supported by the Office of Science of the Department of Energy under Contract No. DE-AC05-00OR22725. The authors would like to thank G. R. Tynan, D. R. Ernst, D. R. Mikkelsen, W. M. Nevins, G. W. Hammett, and P. B. Snyder for many useful discussions.

[1]W. Horton, Rev. Mod. Phys. **71**, 735 (1999).
[2]P. J. Roache, *Verification and Validation in Computational Science and Engineering* (Hermosa, Albuquerque, 1998).
[3]W. L. Oberkampf and M. F. Barone, J. Comput. Phys. **217**, 5 (2006).
[4]P. W. Terry, M. Greenwald, J.-N. Leboeuf, G. R. McKee, D. R. Mikkelsen, W. M. Nevins, D. E. Newman, D. P. Stotler, Task Group on Verification and Validation, U.S. Burning Plasma Organization, and U. S. Transport Task Force, Phys. Plasmas **15**, 062503 (2008).
[5]M. Greenwald, Phys. Plasmas **17**, 058101 (2010).
[6]J. W. Connor, Plasma Phys. Controlled Fusion **37**, A119 (1995).
[7]J. Candy and R. E. Waltz, Phys. Rev. Lett. **94**, 045001 (2003).
[8]D. W. Ross, R. V. Bravenec, W. Dorland, M. A. Beer, G. W. Hammett, G. R. McKee, R. J. Fonck, M. Murakami, K. H. Burrell, G. L. Jackson, and G. M. Staebler, Phys. Plasmas **9**, 177 (2002).
[9]D. W. Ross and W. Dorland, Phys. Plasmas **9**, 5031 (2002).
[10]A. E. White, L. Schmitz, G. R. McKee, C. Holland, W. A. Peebles, T. A. Carter, M. W. Shafer, M. E. Austin, K. H. Burrell, J. Candy, J. C. DeBoo, E. J. Doyle, M. A. Makowski, R. Prater, T. L. Rhodes, G. M. Staebler, G. R. Tynan, R. E. Waltz, and G. Wang, Phys. Plasmas **15**, 056116 (2008).
[11]A. Casati, T. Gerbaud, P. Hennequin, C. Bourdelle, J. Candy, F. Clairet, X. Garbet, V. Grandgirad, O. D. Gürcan, S. Heuraux, G. T. Hoang, C. Honoré, F. Imbeaux, R. Sabot, Y. Sarazin, L. Vermare, and R. E. Waltz, Phys. Rev. Lett. **102**, 165005 (2009).
[12]C. Holland, A. E. White, G. R. McKee, M. W. Shafer, J. Candy, R. E. Waltz, L. Schmitz, and G. R. Tynan, Phys. Plasmas **16**, 052301 (2009).
[13]L. Lin, M. Porkolab, E. M. Edlund, J. C. Rost, M. Greenwld, N. Tsujii, J. Candy, R. E. Waltz, and D. R. Mikkelsen, Plasma Phys. Controlled Fusion **51**, 065006 (2009).
[14]L. Lin, M. Porkolab, E. M. Edlund, J. C. Rost, C. L. Fiore, M. Greenwald, Y. Lin, D. R. Mikkelsen, N. Tsujii, and S. J. Wukitch, Phys. Plasmas **16**, 012502 (2009).
[15]A. E. White, W. A. Peebles, T. L. Rhodes, C. H. Holland, G. Wang, L. Schmitz, T. A. Carter, J. C. Hillesheim, E. J. Doyle, L. Zeng, G. R. McKee, G. M. Staebler, R. E. Waltz, J. C. DeBoo, C. C. Petty, and K. H. Burrell, Phys. Plasmas **17**, 056103 (2010).
[16]J. C. DeBoo, C. Holland, T. L. Rhodes, L. Schmitz, G. Wang, A. E. White, M. E. Austin, E. J. Doyle, J. C. Hillesheim, W. A. Peebles, C. C. Petty, Z. Yan, and L. Zeng, Phys. Plasmas **17**, 056105 (2010).
[17]T. M. Antonsen and B. Lane, Phys. Fluids **23**, 1205 (1980).
[18]E. A. Frieman and L. Chen, Phys. Fluids **25**, 502 (1982).
[19]H. Sugama and W. Horton, Phys. Plasmas **5**, 2560 (1998).
[20]J. Candy and R. E. Waltz, J. Comput. Phys. **186**, 545 (2003).
[21]J. Candy and E. Belli, "GYRO Technical Guide," General Atomics Technical Report GA-A26818, 2010; http://www.fusion.gat.com/theory/GYRO.
[22]J. E. Kinsey, R. E. Waltz, and J. Candy, Phys. Plasmas **14**, 102306 (2007).
[23]G. M. Staebler, J. E. Kinsey, and R. E. Waltz, Phys. Plasmas **14**, 055909 (2007).
[24]J. E. Kinsey, G. M. Staebler, and R. E. Waltz, Phys. Plasmas **15**, 055908 (2008).
[25]C. M. Greenfield, K. H. Burrell, J. C. DeBoo, E. J. Doyle, B. W. Stallard, E. J. Snyakowski, C. Fenzi, P. Gohil, R. J. Groebner, L. L. Lao, M. A. Makowski, G. R. McKee, R. A. Moyer, C. L. Rettig, T. L. Rhodes, R. I. Pinsker, G. M. Staebler, W. P. West, and the DIII-D Team, Phys. Rev. Lett. **86**, 4544 (2001).
[26]K. H. Burrell, W. P. West, E. J. Doyle, M. E. Austin, T. A. Casper, P. Gohil, C. M. Greenfield, R. J. Groebner, A. W. Hyatt, R. J. Jayakumar, D. H. Kaplan, L. L. Lao, A. W. Leonard, M. A. Makowsski, G. R. McKee, T. H. Osborne, P. B. Snyder, W. M. Solomon, D. M. Thomas, T. L. Rhodes, E. J. Strait, M. R. Wade, G. Wang, and L. Zeng, Phys. Plasmas **12**, 056121 (2005).
[27]T. C. Luce, C. C. Petty, and J. E. Kinsey, in *Proceedings of the 28th European Physical Society Conference on Controlled Fusion and Plasma Physics*, *Funchal*, 2001, (EPS, Geneva, 2001), Vol. 25A, p. 1377.
[28]ITER Physics Expert Groups on Confinement and Transport and Confinement Modeling and Database, ITER Physics Basis Editors, and ITER EDA, Nucl. Fusion **39**, 2175 (1999).
[29]C. C. Petty, Phys. Plasmas **15**, 080501 (2008).
[30]G. R. McKee, R. J. Fonck, D. K. Gupta, D. J. Schlossberg, M. W. Shafer, R. L. Boivin, and W. M. Solomon, Plasma Fusion Res. **2**, S1025 (2007).
[31]A. E. White, L. Schmitz, W. A. Peebles, T. A. Carter, T. L. Rhodes, E. J. Doyle, P. A. Gourdain, J. C. Hillesheim, G. Wang, C. Holland, G. R. Tynan, M. E. Austin, G. R. McKee, M. W. Shafer, K. H. Burrell, J. Candy, J. C. DeBoo, R. Prater, G. M. Staebler, R. E. Waltz, and M. A. Makowski, Rev. Sci. Instrum. **79**, 103505 (2008).
[32]R. L. Miller, M. S. Chu, J. M. Greene, Y. R. Lin-Liu, and R. E. Waltz, Phys. Plasmas **5**, 973 (1998).
[33]H.E. St. John, T. S. Taylor, Y. R. Lin-Liu, and A. D. Turnbull, Plasma Phys. Controlled Nucl. Fusion Res. **3**, 603 (1994).
[34]G. G. Lister, D. E. Post and R. Goldston, in *Proceedings of the third Symposium on Plasma Heating in Toroidal Devices, Varenna, 1974* (Editrice Compositori, Bologna, 1974), p. 303.
[35]J. Candy, R. E. Waltz, and W. Dorland, Phys. Plasmas **11**, L25 (2004).
[36]R. V. Bravenec and W. M. Nevins, Rev. Sci. Instrum. **77**, 015101 (2006).
[37]D. R. Ernst, N. Basse, W. Dorland, C. L. Fiore, L. Lin, A. Long, M. Porkolab, K. Zeller, and K. Zhurovich, in *Proceedings of the 22nd IAEA*

Fusion Energy Conference, Chengdu, China, 2006, Paper IAEA-CN-149/TH/1-3.
[38]A. Pankin, D. McCune, R. Andre, G. Bateman, and A. Kritz, Comput. Phys. Commun. **159**, 157 (2004).
[39]F. L. Hinton and R. E. Waltz, Phys. Plasmas **13**, 102301 (2006).
[40]A. M. Dimits, G. Bateman, M. A. Beer, B. I. Cohen, W. Dorland, G. W. Hammett, C. Kim, J. E. Kinsey, M. Kotschenreuther, A. H. Kritz, L. L. Lao, J. Mandrekas, W. M. Nevins, S. E. Parker, A. J. Redd, D. E. Shumaker, R. Sydora, J. Weiland, Phys. Plasmas **7**, 969 (2000).
[41]D. R. Baker, C. M. Greenfield, K. H. Burrell, J. C. DeBoo, E. J. Doyle, R. J. Groebner, T. C. Luce, C. C. Petty, B. W. Stallard, D. M. Thomas, and M. R. Wade, Phys. Plasmas **8**, 4128 (2001).
[42]P. Mantica, D. Strintzi, T. Tala, C. Giroud, T. Johnson, H. Leggate, E. Lerche, T. Loarer, A. G. Peeters, A. Salmi, S. Sharapov, D. Van Eester, P. C. de Vries, L. Zabeo, and K. D. Zastrow, Phys. Rev. Lett **102**, 175002 (2009).
[43]F. Ryter, C. Angioni, A. G. Peeters, F. Leuterer, H.-U. Fahrbach, and W. Suttrop, Phys. Rev. Lett. **95**, 085001 (2005).
[44]R. E. Waltz, J. Candy, and C. C. Petty, Phys. Plasmas **13**, 072304 (2006).
[45]J. Candy, C. Holland, R. E. Waltz, M. R. Fahey, and E. Belli, Phys. Plasmas **16**, 060704 (2009).
[46]R. E. Waltz, J. Candy, F. L. Hinton,C. Estrada-Mila, and J. E. Kinsey, Nucl. Fusion **45**, 741 (2005).
[47]C. Estrada-Mila, J. Candy, and R. E. Waltz, Phys. Plasmas **13**, 112303 (2006).
[48]K. H. Burrell, T. H. Osborne, P. B. Snyder, W. P. West, M. E. Fenstermacher, R. J. Groebner, P. Gohil, A. W. Leonard, and W. M. Solomon, Nucl. Fusion **49**, 085024 (2009).
[49]P. H. Diamond, S.-I. Itoh, K. Itoh, and T. S. Hahm, Plasma Phys. Controlled Fusion **47**, R35 (2005).
[50]C. Holland, G. R. Tynan, R. J. Fonck, G. R. McKee, J. Candy, and R. E. Waltz, Phys. Plasmas **14**, 056112 (2007).